Journal Pre-proof

Performance of cuprous oxide mesoparticles with different morphologies as catalysts in a carbon nanotube ink for printing electrochemical sensors

Lionel S. Veiga, Octavio Garate, Pablo Tancredi, Leandro N. Monsalve, Gabriel Ybarra

PII: S0925-8388(20)32813-9

DOI: https://doi.org/10.1016/j.jallcom.2020.156449

Reference: JALCOM 156449

To appear in: *Journal of Alloys and Compounds*

Received Date: 9 May 2020

Revised Date: 20 June 2020

Accepted Date: 16 July 2020

Please cite this article as: L.S. Veiga, O. Garate, P. Tancredi, L.N. Monsalve, G. Ybarra, Performance of cuprous oxide mesoparticles with different morphologies as catalysts in a carbon nanotube ink for printing electrochemical sensors, *Journal of Alloys and Compounds* (2020), doi: https://doi.org/10.1016/j.jallcom.2020.156449.

Credit Author Statement

Lionel S. Veiga: Conceptualization (Synthesis), Methodology, Investigation (Synthesis and Materials Characterization), Visualization, Writing - Original Draft.

Octavio Garate: Conceptualization (Synthesis), Methodology, Investigation (Electrochemical Sensors), Visualization, Writing - Original Draft.

Pablo Tancredi: Investigation (Materials Characterization), Writing - Review & Editing.

Leandro N. Monsalve: Conceptualization (CNT inks), Investigation (CNT inks), , Writing - Review & Editing. Funding acquisition.

Gabriel Ybarra: Conceptualization (Electrochemical Sensors), Visualization, Writing - Review & Editing, Supervision. Funding acquisition.

		N_2H_4:$CuCl_2$					
		1	2	3	4	5	10
NaOH:$CuCl_2$	0	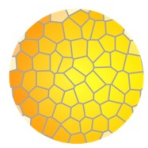	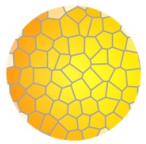	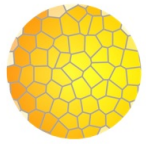	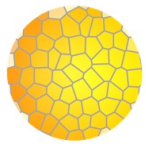	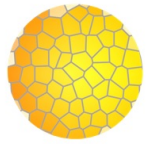	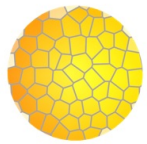
	1	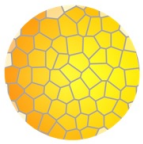	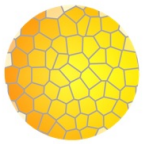	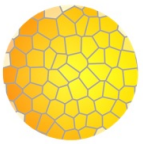	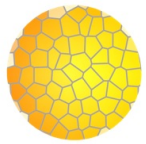	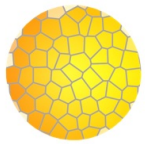	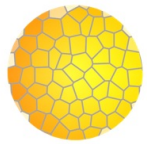
	2	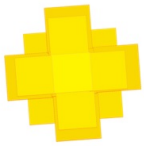				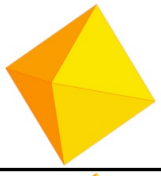	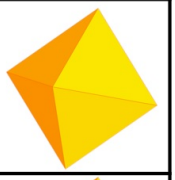
	5	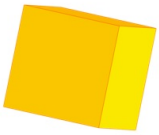					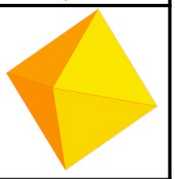
	10	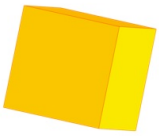				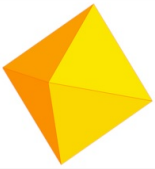	

Performance of Cuprous Oxide Mesoparticles with Different Morphologies as Catalysts in a Carbon Nanotube Ink for Printing Electrochemical Sensors

Lionel S. Veiga,[1,*] Octavio Garate,[1] Pablo Tancredi,[1,2] Leandro N. Monsalve,[1,2] Gabriel Ybarra[1]

[1] Nanomateriales Funcionales, INTI-Micro y Nanotecnologías, Instituto Nacional de Tecnología Industrial, San Martín, Buenos Aires, Argentina.

[2] CONICET.

*Corresponding author: lveiga@inti.gob.ar

Abstract

A simplified, surfactant-free method is presented for the synthesis of cuprous oxide mesoparticles involving the use of only three reactants at room temperature. Different morphologies, such as cubes, cuboctahedra, truncated octahedra, octahedra, hexapods, and porous spheres could be obtained using different concentrations of reactants. The roles played by each reactant in the synthesis are critically discussed. The mesoparticles were used in the formulation of carbon nanotube-based waterborne inks to prepare coated electrodes. The electrocatalytic activity of the different cuprous oxide mesoparticles used in the inks towards hydrogen peroxide reduction was measured and compared. Cuprous oxide hexapods yielded the highest sensitivity whereas porous spheres were superior in terms of stability. The combination of carbon nanotubes and cuprous oxide mesoparticles in waterborne ink allows printing of electrodes combining electrical conduction and electrocatalysis in a single layer printed onto flexible substrates.

Keywords: Carbon Nanotubes Ink; Copper Oxide Particles; Electrocatalysis.

Graphical Abstract

1. Introduction

Controlling the shape and size of inorganic crystals has been one of the main goals of material scientists during the last decades. Both characteristics define the nature of the exposed surface and the facets, affecting the electronic structure and surface energy of the crystals, and therefore their catalytic and sensing properties. Generally speaking, crystals with high-index facets commonly present better catalytic performance [1], but their low stability, as well as their challenging synthetic procedures, hinder its use in different technological applications [2]. On the other hand, crystals with low-index facets, such as {100}, {110} and {111}, have both acceptable catalytic activity and excellent stability, turning them into suitable candidates in sensing and catalytic applications.

Among the vast number of materials with shape-dependent properties, the inexpensive, non-toxic and abundant cuprous oxide crystals have been widely studied due to its interesting catalytic activity, with extensive applications in gas sensors [3], electrochemical sensors [4-6], photocatalysis [7], carbon dioxide reduction [8], water splitting [9], and organic catalyzers [10,11]. Since the pioneering work by Matijevic in 1972 [12], many synthetic routes of Cu_2O crystals with different and well-defined shapes have been developed. The foremost extended strategies employ organic surfactants (PVP [13, 14], PEG [15], CTAB [16], and SDS [17, 18]) during the crystal synthesis, which selectively modify the surface energy of specific facets. Facets with the lowest surface energy are favoured during the crystal growth, promoting the formation of octahedral or cubic crystal habits depending on the case. However, the inclusion of these additives introduces additional complexity in deciphering the growth mechanism, and also may affect the catalytic performance of the system. Several researchers have reported the preparation of well-defined crystals through surfactant-free synthesis, by varying the type and the amount of the reducing agent (ascorbic acid [9, 17, 18], glucose [19], hydrazine [11, 19, 20], and hydroxylamine [22]), the complexant agent (NH_3 [23, 24], OH^- [19, 20], sodium citrate [25], and EDTA [26]) or the counterion of the copper salt precursor [27]. However, the precise effects of each reagent on the growth process are still not entirely clear. By unravelling the role played by each of them in the growth mechanism behind crystal formation, it could be possible to produce tailored materials with specific physical and chemical properties.

An exciting application of Cu_2O materials is the electrochemical detection of hydrogen peroxide [28]. The quantitative measurement of H_2O_2 is a widely employed strategy used to track the oxidative stress *in vivo* [29]. Moreover, as a by-product of the reaction of the oxidase enzymes, the measurement of H_2O_2 also allows the indirect detection of worthy molecules with biological interest such as glucose and lactate [30-32].

The electrocatalytic performance of Cu_2O crystals of different morphologies has been studied by different authors. For instance, Li at al. [33] reported the electrochemical detection of H_2O_2 by casting Nafion-impregnated hierarchical Cu_2O particles onto a glassy carbon electrode, showing some promising features such as fast response, high sensitivity, low limit of detection and wide linear range. Zhong et al. [18] studied the shape-dependent H_2O_2 sensing properties of several types of Cu_2O particles, finding that the shapes exposing {111} facets presented enhanced sensitivity and limit of detection compared to the shapes with {100} facets.

Although novel Cu_2O-based materials are being continuously reported, their electrocatalytic performance is frequently evaluated in laboratory conditions with mass transport assistance. In this sense, the necessity of developing mass production low-cost sensors with a high sensitivity under purely diffusional conditions is still a challenge to overcome. The fabrication of non-enzymatic sensors by printing techniques could be an affordable solution for the fabrication of scalable and low-cost electrodes [34-36]. Printed electronics allows the fabrication of disposable electroanalytical devices on flexible substrates in large areas which requires conductive inks as basic supplies. Our group has previously reported the development of a waterborne conductive ink based on multiwalled carbon nanotubes (CNTs) which showed electrocatalytic activity and could be used for the fabrication of enzymatic biosensors [37, 38]. The use of waterborne carbon nanotube inks as active materials for these

applications has shown considerable advantages due to its processing ease, high specific surface area and chemical versatility towards functionalization. However, the combination of nanotubes inks with inorganic crystals such as Cu_2O in order to develop improved sensing devices is still a barely explored strategy.

In this work, we present a simplified method for the synthesis of cuprous oxide particles with different morphologies using only three reactants and the role played by each reactant is discussed. The electrocatalytic behaviour towards hydrogen peroxide reduction was evaluated amperometrically using electrodes coated with a CNT ink loaded with the different particles and the obtained results are critically compared with previously reported systems.

2. Experimental

2.1 Synthesis of Cu_2O particles

In a typical synthesis, 0-480 µL of 1 M NaOH were added to 50 ml of 1 mM $CuCl_2$ under vigorous magnetic stirring. Then, 20-200 µL of 2.4 M of hydrazine (N_2H_4) were quickly added to the solution at room temperature. Depending on the reagent's ratios, the solution turned either pale yellow or brick-red, indicating the presence of Cu_2O particles. After 40 minutes, the samples were centrifuged at 6000 rpm for 5 min (Mikro 1200, Hettich) and washed three times with deionized water. Finally, they were dispersed in 1 ml of water. A total of 30 samples were prepared by combining 5 different molar ratios of NaOH:$CuCl_2$ with 6 different molar ratios of N_2H_4:$CuCl_2$. For further identification, the samples were named according to the conditions used in the synthesis. For example, sample 2:4 was prepared with a NaOH:$CuCl_2$ molar ratio of 2 and a N_2H_4:$CuCl_2$ molar ratio of 4.

2.2 Characterization of Cu_2O particles

Scanning electron microscopy (SEM) images were taken with a FEI Quanta 250 after solvent evaporation of drop casted dispersions. X-ray diffraction (XRD) patterns were obtained with a standard Rigaku diffractometer with CuKα radiation.

2.3 Formulation and characterization of inks modified with Cu_2O particles

A 2.5% carbon nanotube waterborne ink was prepared as previously reported [39]. Cu_2O dispersions were mixed with the CNT ink in order to obtain a Cu_2O to CNT mass ratio of 1:1. For the electrochemical measurements, dispersions of Cu_2O, CNT, and the CNT + Cu_2O inks were either drop-casted onto glassy carbon (GC) rotating disk electrodes with a diameter of 5 mm or used to coat Valox™ plastic substrates with a Mayer rod coater (nominal thickness 100 µm), drying the coating at room temperature. A Pt foil with an area of 5 cm^2 was used as counter electrode and a silver/silver chloride electrode (Ag|AgCl|1M KCl) was used as a reference electrode. Electrochemical measurements were carried out using a Teq4 potentiostat (NanoTeq, Argentina). Limits of detection (LOD) were calculated as LOD = $3\delta/m$, where δ was the standard deviation of three voltammetric measurements and m the sensitivity. Surface resistivity measurements were performed by measuring the resistance with a Keithley 2100 digital multimeter equipped with a four-point probe.

3. Results and discussion

3.1 Synthesis and characterization of Cu_2O particles

Cu_2O particles were obtained by the reduction of cupric ions from a solution of $CuCl_2$ with different amounts of N_2H_4 and NaOH, varying the NaOH:$CuCl_2$ and N_2H_4:$CuCl_2$ molar ratios between 0 and 10 and between 1 to 10, respectively~~, as shown in T able 1~~. Particles with different morphologies, such as porous spheres, cubes, cuboctahedra, truncated octahedra, octahedra and hexapods were synthesized without the addition of surfactants. ~~The particles were characterized using scanning electron microscopy (Fig. 1).~~ A selection of several SEM images showing these different shapes are presented in Fig. 1. The particles' size was estimated by measuring at least 100 particles. The diameter was measured in the sphere-shaped particles, while the longest edge lengths were measured in the rest of the morphologies.

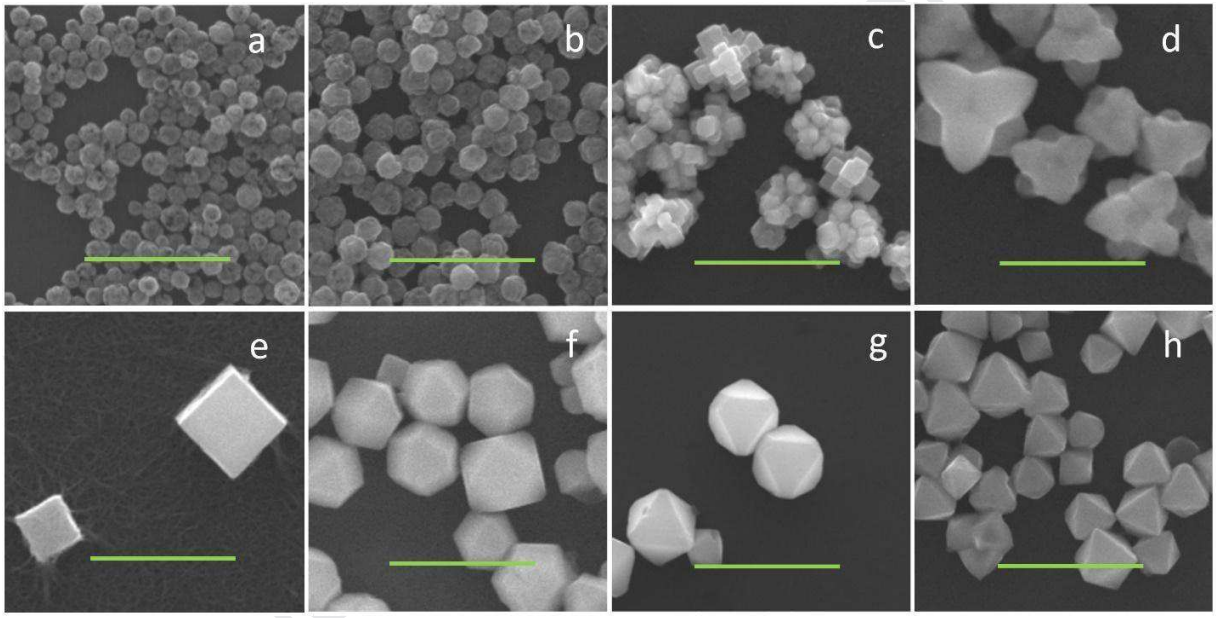

Fig. 1. SEM images of particles of different shape obtained under different synthesis conditions: porous spheres from samples 0:3 and 1:5 (a and b), aggregated cubes from sample 2:1 (c), hexapods from sample 2:3 (d), cubes from sample 5:1 (e), truncated octahedra from sample 5:2 (f), cuboctahedra from sample 5:3 (g) and octahedra from sample 5:4 (h). Bar size: 1 µm.

~~**Fig. 1.** SEM images of the obtained particles under different conditions with different shapes: porous spheres (a and b), aggregated cubes (c), hexapods (d), cubes (e), truncated octahedra and cuboctahedra (f and g) and octahedra (h). Bar size: 1 µm.~~

Both reagents ratios were key factors determining the morphology of the particles. When the NaOH:$CuCl_2$ ratio was below 2, the solution changed from slightly pale blue to intense yellow in less than one minute after adding the reducing agent. Nearly spherical particles with a diameter of approx. 100 nm and a low size dispersion were obtained without the addition of NaOH (Fig. 1.a). As the concentration of N_2H_4 increased without modifying the NaOH:$CuCl_2$ ratio, cuprous oxide particles with a more defined spherical shape were obtained, and their average size increased from 100 to 130 nm.

When NaOH was added to obtain a NaOH:$CuCl_2$ molar ratio of 1, the average size of the cuprous oxide particles increased up to 170 nm (Fig 1.b).

When the NaOH:$CuCl_2$ ratio reached a value of 2 or higher, the solution presented an intense turbid blue color, indicating the formation of $Cu(OH)_2$ colloids and, consequently, the formation of cuprous oxide particles became a slower process. The color change of the preparation from blue to orange/brick red took around 25 minutes. For a NaOH:$CuCl_2$ ratio of 2, aggregated cubes of Cu_2O were obtained if low amounts of N_2H_4 were used (Fig. 1.c), while hexapods (Fig. 1.d) and octahedra of 300-500 nm were obtained by sequentially increasing the N_2H_4 concentration.

Finally, ~~when the NaOH:$CuCl_2$ molar ratio was above 2, SEM images showed well-shaped submicrometric crystals. Cubes, cuboctahedra, truncated octahedra and octahedra were obtained with increasing hydrazine concentration (Fig. 1e-h).~~ the synthesized particles showed well-shaped submicrometric crystals when the NaOH:$CuCl_2$ molar ratio was above 2. Cubes (Fig. 1.e), cuboctahedra (Fig. 1.f), truncated octahedra (Fig. 1.g) and octahedra (Fig. 1.h) can be obtained by changing the concentration of N_2H_4 while keeping the NaOH concentration fixed. Under those conditions, an increase in the particle size was observed with higher NaOH concentrations. Similar results were found in previous works [20, 40], with no significant dependence of the particle size on the concentration of N_2H_4. ~~The different morphologies are schematically shown in Fig. 2, where representative shapes and sizes obtained for each molar ratio of NaOH:$CuCl_2$ and N_2H_4:$CuCl_2$ are displayed.~~ The size and shape evolution from cubes to octahedra for the series with highest NaOH:$CuCl_2$ molar ratio, and from spheres to octahedra for the series with the highest N_2H_4:$CuCl_2$ molar ratio are shown in Fig. 2. The change in the particle shape is also related to the change in the crystallographic planes of the facets, as will be explained later during the discussion of the growth mechanism. The different morphologies obtained under the studied conditions are schematically shown in Fig. 3, where representative shapes and sizes for each molar ratio of NaOH:$CuCl_2$ and N_2H_4:$CuCl_2$ are displayed.

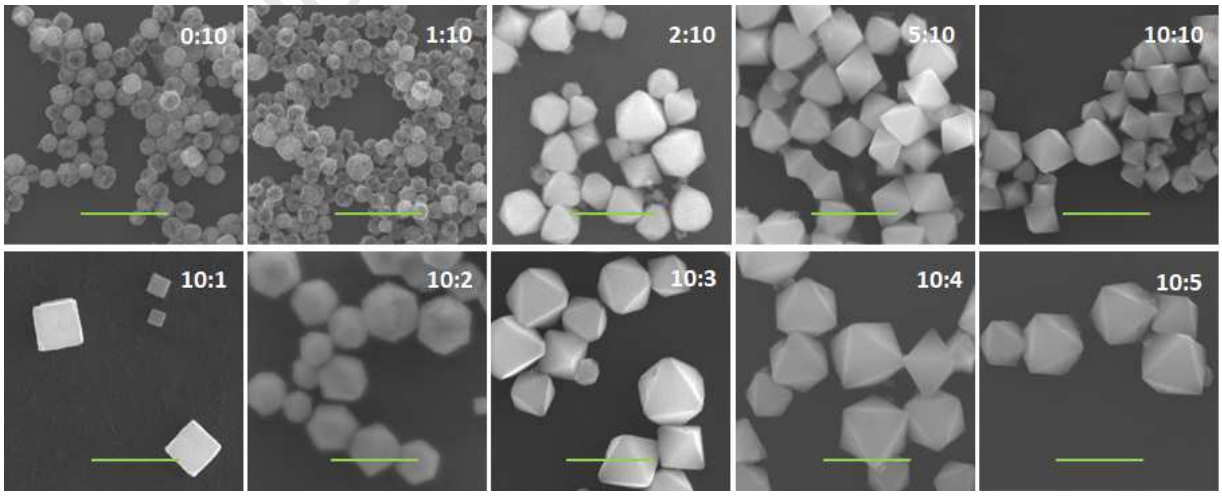

Fig. 2. Size and shape evolution of samples prepared with a fixed N_2H_4:$CuCl_2$ ratio of 10 and variable NaOH:$CuCl_2$ ratios (upper row), and samples prepared with a fixed NaOH:$CuCl_2$ ratio of 10 and variable

N_2H_4:$CuCl_2$ ratios (lower row). Samples are individually identified by name in the SEM image. Bar size: 1 µm.

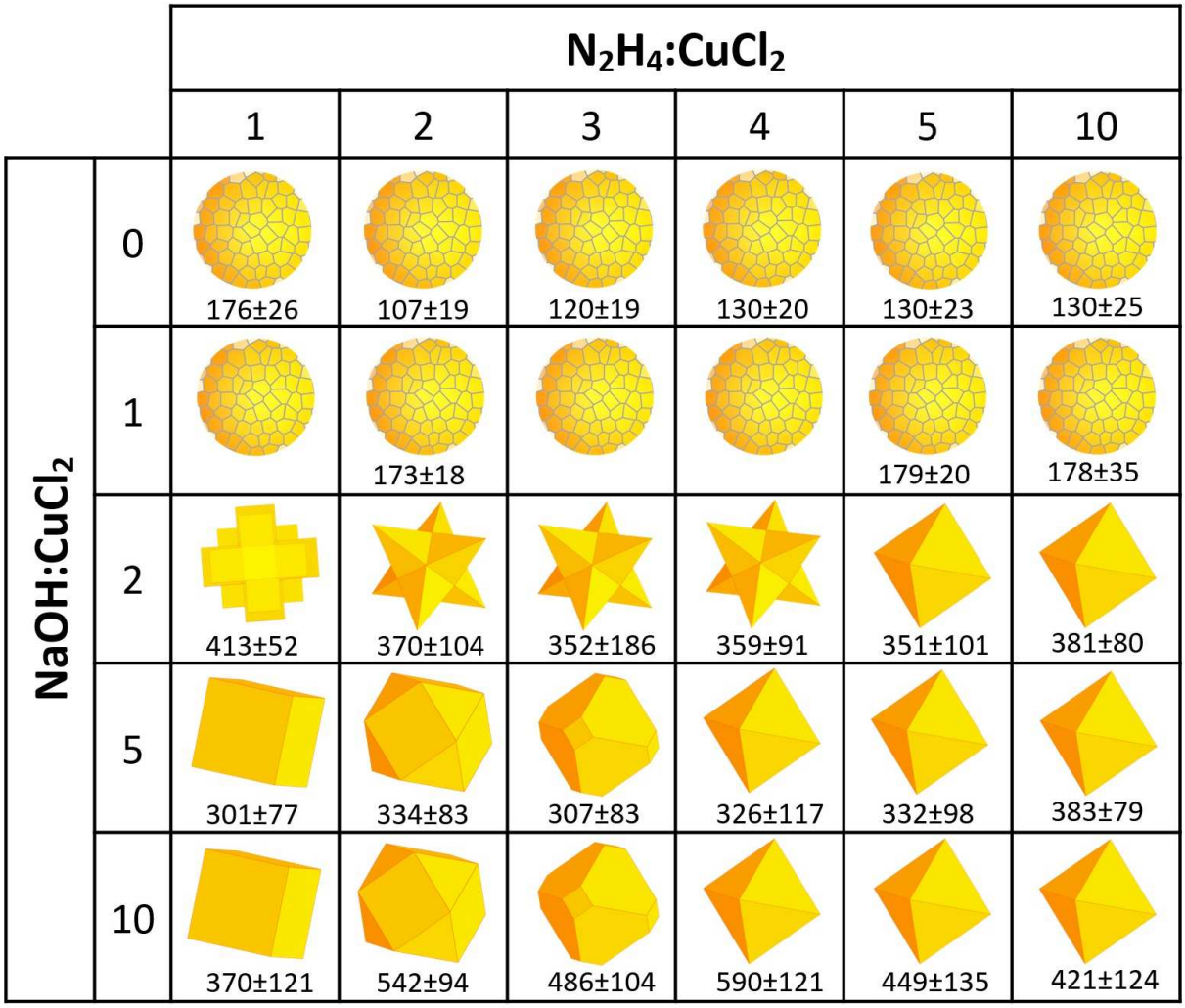

Fig. 3. Schematic representation of morphologies and average diameter obtained under different synthesis conditions.

The phase composition ~~and structure~~ of the particles was evaluated by X-ray diffraction (Fig. 3). ~~Peaks in XRD patterns appeared at 2θ values of 29.5°, 36.3°, 42.2°, and 61.1°. The obtained XRD pattern is consistent with the cubic face structure of Cu_2O crystal, and peaks could be assigned to (110), (111), (200) and (220) planes (JCPDS file No. 05–0667).~~ Despite the differences in shape, the XRD patterns obtained for the different samples are very similar, with an intense peak located at 36.3° and others less intense located at 29.5°, 42.2°, and 61.1°. These patterns are consistent with the cubic-face structure of

Cu_2O crystal (JCPDS file No. 05–0667). No evidence of other phases, such as Cu, CuO or $Cu(OH)_2$, was found in any of the studied systems. The relative intensity variations observed between peaks of the different patterns can be attributed to a preferential orientation of the crystals during the deposition and drying of the suspension over the sample holder. The (111) peak located at 36.3° is notoriously wider for the spheres when compared to the other shapes. Considering the well-known relationship between the peak width and the crystallite size, this observation supports the idea that the Cu_2O spheres are polycrystals composed of dozens of small crystallites, as already suggested by SEM images.

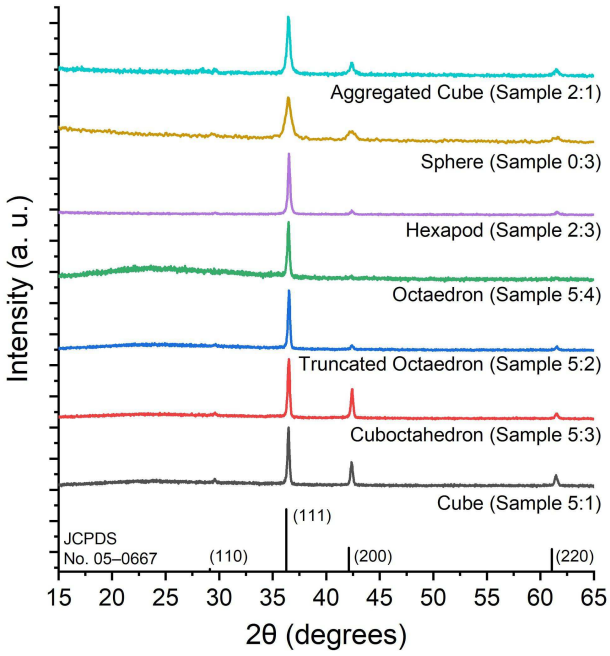

Fig. 4. XRD patterns of the different morphologies of Cu_2O particles.

3.2 Growth mechanism

Cu_2O crystallizes in a simple cubic structure, which can be represented as a tetrahedral array of copper atoms encircling an oxygen atom. This atomic packing leaves each Cu atom neighboring two oxygen atoms. The surface atomic structure of {111} and {100} facets have different crystal arrangements [41]. {100} facets are terminated in O atoms, leading to electric neutrality. By contrast, {111} facets have unsaturated Cu atoms with dangling bonds perpendicular to the surface, providing an overall positive charge. Based on the Gibbs-Wulff theorem, facets with lower surface energies grow more slowly and are conserved in the final structure. In the case of Cu_2O, the surface energy of {100} facets are lower than the energy of {111} facets [42]. However, this situation could be modified through the addition of inorganic or organic compounds with the capability of interacting selectively with each facet, modifying the relative order of surface energy of the facets and inducing changes in crystal morphology. It is worth noting that cubic Cu_2O crystals exhibit only {100} facets and octahedral crystal only {111} facets, while

cuboctahedra exhibit both {100} and {111} facets. The wide variety Cu_2O morphologies obtained, shown in Fig. 1 and 3, can be explained by the effects of the different ions and molecules, such as OH^- and N_2H_4, on the different facets.

The obtention of various morphologies with the use of only three reactants indicates that each reagent may play more than one role in the synthesis. For instance, N_2H_4 is a reducing agent which may also selectively interact with the different crystalline facets and thus influence the final morphology. N_2H_4 is also an O_2 scavenger. When enough N_2H_4 is present in the reaction media, dissolved O_2 is effectively removed. Under those conditions, the obtained microcrystals are equivalent to those obtained under an inert atmosphere. However, when N_2H_4 concentration is not high enough to remove O_2, oxidative etching can take place.

Similarly, hydroxide ions can react with cupric ions promoting the formation of $Cu(OH)_2$, which reduces the concentration of Cu(II) ions and thus slows down the reaction kinetics. However, OH^- ions also interact selectively with the Cu_2O facets influencing the resulting morphology.

The molar ratio of Cu(II) ions and OH^- determines the initial concentration of a Cu ions in solution. For a NaOH:$CuCl_2$ molar ratio ~~equal to or~~ higher than 2, most of the Cu(II) ion is in the form of $Cu(OH)_2$ in equilibrium with a low concentration of Cu(II) ions in solution. $Cu(OH)_2$ acts as a reservoir of Cu(II) ions, decreasing ~~diminishing~~ the reaction rate for the reduction. Under these conditions, well-defined crystals with sharp faces were formed, indicating a selective growth of the crystal facets {100} and {111} as shown in the cube-cuboctahedron-octahedron transition. Previous works were able to control the growth of both crystal facets through the addition of surfactants such as PVP [13] or NH_3 [24], which reduce the surface energy of {111} facets and hence octahedra were obtained. On the other hand, molecules with carbonyl functional groups like sodium citrate lead to crystal growth through {100} facet and consequently cubic particles were obtained [25]. Ascorbic acid could lead to the growth of cubes due to {100} facets stabilization, while N_2H_4 was shown to stabilize {111} facets [19, 20]. The surfactant-free synthesis presented here was capable of controlling the growth rate through only the increase of the N_2H_4 concentration.

~~By varying the N_2H_4 concentration, it was possible to control precisely the growth of {111} facets, thus obtaining cuboctahedra and truncated octahedra. To corroborate that no other directing agent was present, complementary experiments were carried out.~~ Complementary experiments were carried out to corroborate that no other directing agents were involved in the reaction. ~~Firstly~~ First, $CuCl_2$ was replaced with $Cu(NO_3)_2$ and $CuSO_4$ to assess the counterion effect~~. As can be seen in Suppl. Info. Fig. S1 and S2, no further modification in the crystal morphology was observed.~~, and no significant modification in the crystal morphology was observed due to these changes (Suppl. Info, Fig. S1 and S2). ~~A second consideration was the possible etching effect of dissolved oxygen over {111} facets. The same condition for cube synthesis was carried out in a N_2 atmosphere and no crystal morphology alteration was observed (Suppl. Info, Fig. S3). Both experiments suggest that, under those conditions,~~ A second consideration was the effect of dissolved O_2. The same conditions for cubes and octahedra synthesis was carried out in a N_2 atmosphere and no alteration of the crystal morphology was observed (Suppl. Info, Fig. S3 and S4). Both experiments suggest that under high NaOH concentrations the morphology was determined only by the concentration of N_2H_4. When the N_2H_4:$CuCl_2$ ratio was 1, no significant excess of N_2H_4 was available for adsorption, which resulted in the formation of cubic crystals. When the

concentration of N_2H_4 was increased, cuboctahedral and truncated octahedral particles were obtained. Adsorption led to lowering the surface energy of {111} facets and the growth of both facets was similarly promoted. When the N_2H_4:$CuCl_2$ ratio was higher than 4, only octahedra were synthesized.

When a NaOH:$CuCl_2$ ratio of 2 was used, low N_2H_4 concentrations induced the formation of aggregated cubes and hexapods while at higher concentrations, only octahedra were obtained. The formation of hexapods can be attributed to an etching process by O_2 over the {111} facets, as previously reported by Sun et al [43]. T~~o confirm this hypothesis, the synthesis was carried out in N_2 atmosphere, keeping unaltered the rest of the synthetic conditions in which hexapods were obtained. As it is shown in Fig. S4 (Suppl. Info.), octahedra were obtained in N_2 atmosphere, confirming O_2 etching. When the concentration of N_2H_4 was increased, O_2 etching was not further relevant, because N_2H_4 in excess chemically produced a deoxygenated solution.~~ Fig. 5 presents the evolution from hexapods to octahedra of selected particles from samples prepared with a NaOH:$CuCl_2$ ratio of 2, showing how the etching process loses strength as the N_2H_4:$CuCl_2$ ratio increases. This trend is caused by excess N_2H_4 reacting with the dissolved O_2 and leading to a chemically deoxygenated solution. In this sense, O_2 etching was found to be significant only at a low-to-medium N_2H_4:$CuCl_2$ ratio and a medium NaOH:$CuCl_2$ ratio. To confirm this hypothesis, the synthesis of sample 2:2 was carried out under a N_2 atmosphere, keeping unaltered the rest of the synthetic conditions. The particles produced under these conditions were octahedra, confirming the O_2 etching process (Suppl. Info, Fig. S5).

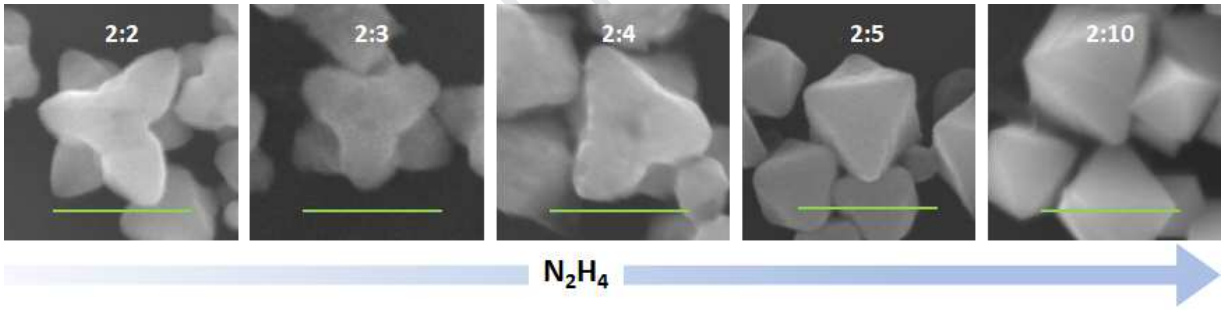

Fig. 5. Evolution from hexapods to octahedra due to distinct O_2 etching of selected particles from samples prepared with a fixed NaOH:$CuCl_2$ ratio of 2 and variable ratios N_2H_4:$CuCl_2$. Bar size: 500 nm.

The pH of the Cu^{2+} solution after NaOH addition was measured to clearly understand the effect of OH^- in the crystal formation. The titration curve of this experiment is presented in Fig. 6. Initially, the gradual addition of NaOH produces the precipitation of $Cu(OH)_2$ colloids, and the pH values slightly shift due to the buffer effect of $Cu(OH)_2$. Immediately after reaching the stoichiometric equivalence (NaOH:$CuCl_2$ ratio of 2) a steep shift in the pH solution was observed. The samples obtained at different pH values present clear morphologies differences. For instance, when employing a fixed N_4H_2:$CuCl_2$ ratio of 3, spheres were synthesized at pH values near 7.0 and below the stoichiometric conditions (sample 1:3), hexapods were obtained at pH values slightly above 7.0 at the stoichiometric equivalence (sample 2:3), and octahedra were synthesized at pH values higher than 11 in the presence of excess OH^- (sample 5:3 and 10:3). As mentioned before, {111} facets have a positive surface charge, with local dangling bonds

that can easily interact with negative ions such as OH^-. As the OH^- concentration increases, {111} facets are protected and no further O_2 etching can take place [25].

~~The addition of NaOH produced the formation of Cu(OH)2 colloids, followed by an increment in pH (Fig. 4). Below the stoichiometric ratio between NaOH and CuCl2, there was a slight pH modification due to the buffer effect of Cu(OH)2. When NaOH:CuCl2 ratio was higher than 2 and the stoichiometric relation was exceeded, a steep shift in pH was observed. As shown by Ho et al. [5], the modification in the pH led to the formation of different hexapods. As mentioned before, {111} facets have a positive surface charge and interact with ions less strongly in the center of the facets, which are therefore more prone to oxygen etching. As it can be seen in the Suppl. Info. (Fig. S5), when the pH was 8.34 defined hexapods appeared. When pH was higher than 11, octahedra were obtained, possibly because OH- protects the whole crystal and no effects of oxygen etching were observed.~~

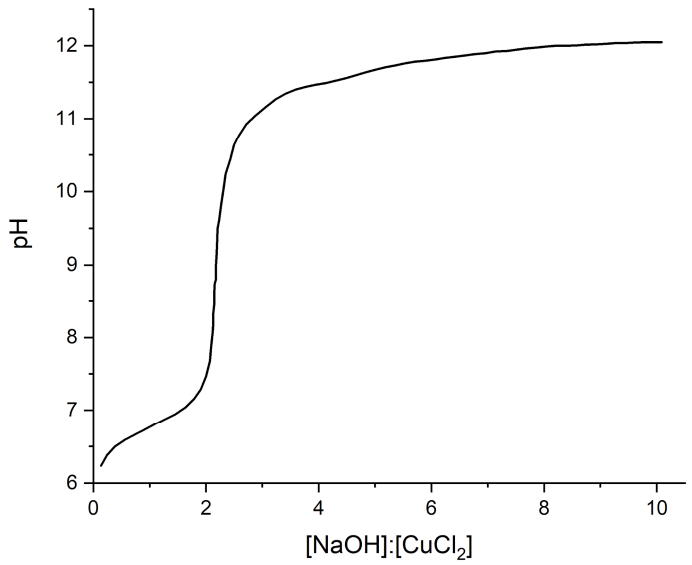

Fig. 6. Evolution of the resulting initial pH of the reaction mix as a function of the $NaOH:CuCl_2$ ratio.

For a $NaOH:CuCl_2$ molar ratio lower than 2, relatively high concentrations of Cu(II) ions were available in the solution. Therefore, the reduction of Cu(II) ions was fast. Under these conditions, monodisperse porous spheres were synthesized. Zhang et al. [44] proposed a mechanism for the synthesis of porous spheres in which small Cu_2O crystallites are first formed, followed by an aggregation process. Solid particles in the inner core have a higher surface energy than those located in the outer core leading to symmetric hollowing during Ostwald ripening. This favors the dissolution of the inner particles, generating cavities inside the aggregated particle. Therefore, quasi-spherical porous particles were produced. When a sub-stoichiometric amount of NaOH was added, the Cu_2O particles tended to be larger and less porous. This can be attributed to a two-step process, in which nucleation and aggregation of small particles from the reduction of free Cu(II) are followed by growth at the expense of the $Cu(OH)_2$ colloid.

3.3 Electrocatalysis of hydrogen peroxide reduction

The catalytic properties towards hydrogen peroxide reduction and the stability of the different cuprous oxide nanoparticles were evaluated. This was performed by preparing electrodes from a mixture of a waterborne CNT ink with the addition of cuprous oxide particles of different shapes.

Fig. 7 displays the cyclic voltammograms obtained at pristine and coated GC electrodes in a 0.1 M phosphate buffer solution of pH 7.4. While a bare GC electrode and a CNT coated one displayed a capacitive behavior, it could be noted that the current for the latter was considerably higher than the uncoated electrode. On the other hand, the effect of Cu_2O particles drop-casted onto a GC electrode showed redox peaks between -0.2 and 0.1 V. These anodic and cathodic peaks could be assigned to the oxidation of Cu_2O to CuO and the further reduction of CuO to Cu_2O. As expected, the printed electrode of CNT-Cu_2O particles showed both capacitive and redox behavior.

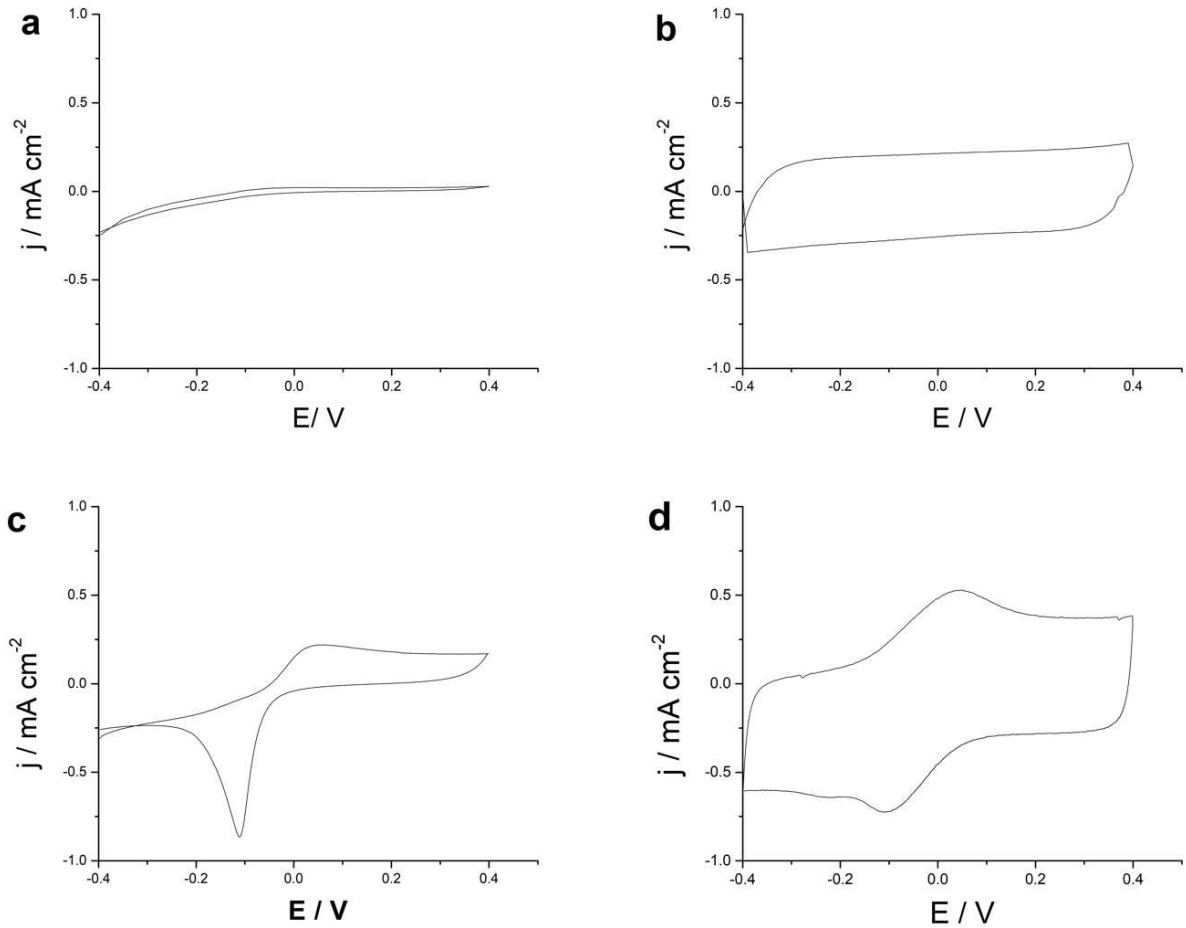

Fig. 7. Cyclic voltammogram obtained at a glassy carbon electrode (a), a CNT ink coated electrode (b), a Cu_2O spheres coated electrode (c) and a CNT ink + Cu_2O spheres from sample 0:3 coated electrode (d) in 0.1M phosphate buffer solution of pH 7.4 at a scan rate of 0.05 V s^{-1}.

Fig. 8a and 8b show current-potential curves at a scan rate of 0.05 V s^{-1} of 0.1M phosphate buffer solution of pH 7.4 at CNT and CNT + Cu_2O spheres ink coated Valox™ electrodes with different

concentrations of H_2O_2 (0, 0.3, 0.6, 1, 2, 5, 8 and 10 mM). For all the morphologies involved, cuprous oxide-based inks showed a linear current-concentration response (Fig. 8c). Sensitivity and limits of detection for each morphology in quiescent solutions are summed up in Table 1. ~~while linear plots of current measured at -0.4 V vs H2O2 concentration are displayed in Suppl. Info. (Fig. S5).~~

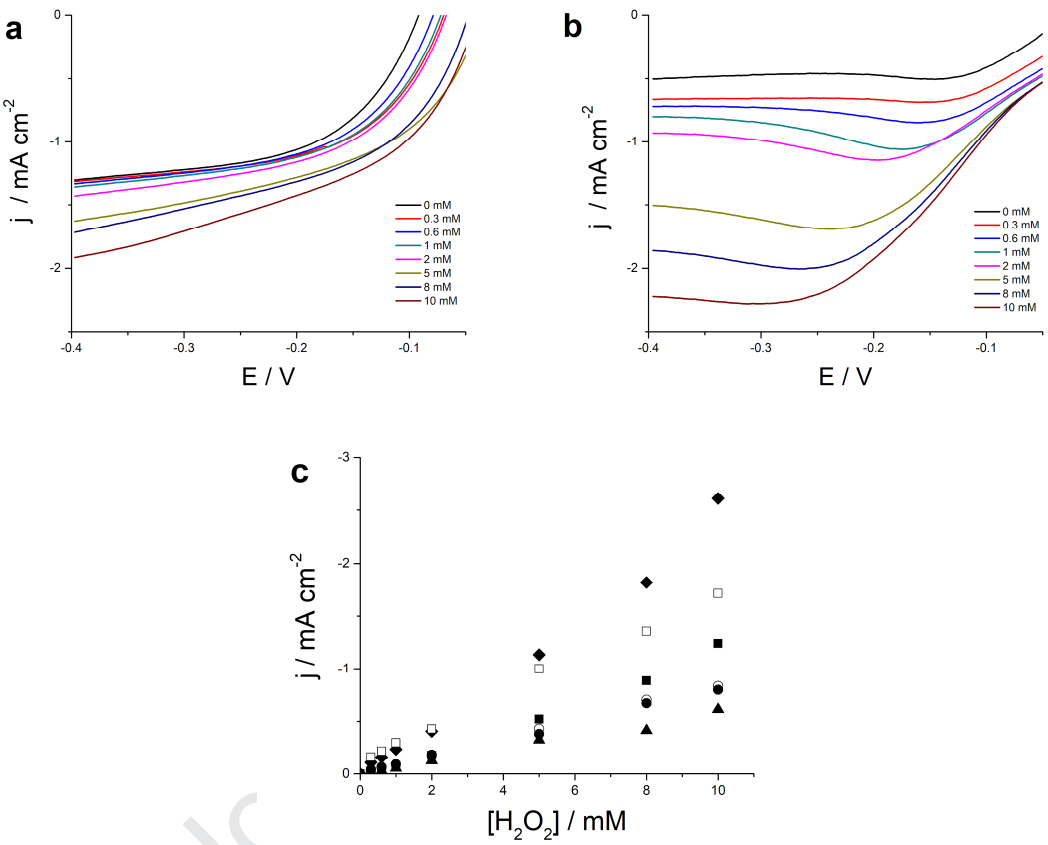

Fig. 8. Current-potential curves at a scan rate of 0.05 V s^{-1} of CNT (a) and CNT + Cu_2O spheres (b) ink coated Valox™ electrodes in 0.1M phosphate buffer solution of pH 7.4 with different H_2O_2 concentrations (0, 0.3, 0.6, 1, 2, 5, 8 and 10 mM). ~~(c) Dependence of current density measured at -0.4 V with hydrogen peroxide concentration for CNT (open circles) and CNT + Cu_2O spheres (full circles) printed electrodes~~. (c) Dependence of the increment in current density measured at -0.4 V with H_2O_2 concentration for CNT (triangles) and CNT + Cu_2O ink coated Valox™ electrodes presented for each cuprous oxide morphology in quiescent solutions for hexapods (full diamonds), spheres (open squares), octahedrons (full squares), cuboctahedrons (open circles), cubes (full circles).

As it was previously reported [7, 18], {111} facets present a higher electrocatalytic activity than {100} facets, which explains ~~the trend in decreasing sensitivity~~ the decreasing trend observed for the electrochemical performance of the cube-cuboctahedron-octahedron sequence. This phenomenon can be attributed to some specific features of the {111} facets such as the higher surface energy and the unsaturated coordination of Cu atoms that leads to dangling bonds perpendicular to the surface.

Furthermore, {111} facets present a positive charge while {100} facets are electrically neutral, allowing them to easily interact with polarizable molecules such as H_2O_2 [13, 42]. The high sensitivity and low limit of detection measured for spherical Cu_2O particles can be attributed to a relatively high surface energy that is related to the small crystallite size of the nanocrystals that conforms the mesoporous structure.

Finally, ink-coated Valox™ electrodes were prepared. The printed layer showed a surface resistivity of 171 ± 20 Ω/□. Stability tests were performed by determining the sensitivity and LOD daily over a two-week period (Table 2). To avoid any unwanted reaction during the process such as oxidation or precipitation of salts, after each measurement the electrodes were rinsed with distilled water to remove phosphate salts remaining on their surface and kept dry avoiding any light source. Expressed as a sensitivity loss percentage in Table 2, the results have shown that after two weeks Cu_2O spheres is the most stable morphology in terms of sensitivity, losing only 10 % of its catalytic activity. Other morphologies such as hexapods, octahedron and cuboctahedron present a 35-50 % activity loss while cubes only retain 9% of its original catalytic activity. While the reason for this sensitivity loss can be attributed to the dissolution of particles from the electrode to the buffer solution, further studies are required to confirm this hypothesis.

Sensitive Layer	Sensitivity (μA cm^{-2} mM^{-1})	LOD (mM)	% Sensitivity loss (14 days)
Hexapods	247	0.13	50
Sphere	162	0.05	10.1
Octahedron	121	0.14	38
Cuboctahedron	84	0.25	47
Cube	79	0.45	91

Table 1. Analytical performance of CNT + Cu_2O ink coated Valox™ electrodes towards hydrogen peroxide reduction presented for each cuprous oxide morphology in quiescent solutions.

In comparison to similar systems in which catalytic inorganic particles were added to a CNT matrix for the amperometric determination of hydrogen peroxide, cuprous oxide-CNT printed electrodes showed a higher sensitivities and lower limits of detection (Table 2). Due to the different hydrodynamic conditions used for the determination of sensitivity, comparisons with previous reported non-enzymatic sensors are not always straightforward. In quiescent solutions, electrodes prepared with CNT-based inks with Cu_2O spheres presented a sensitivity of 162 μA cm^{-2} mM^{-1} and a limit of detection of 50 μM. On the other hand, glassy carbon rotating disk electrodes coated with the same ink presented a sensitivity of 642 μA cm^{-2} mM^{-1} and limit of detection of 1 μM at 800 RPM, respectively (Suppl. Info, Fig. S6). Despite the improvements in sensitivity and LOD observed under forced convection, results under purely diffusional conditions should be considered for applications such as wearable sensors.

Electrode	Sensitivity ($\mu A\ cm^{-2}\ mM^{-1}$)	Linear range (mM)	Detection limit (µM)	Reference
Cu_2O/PANI/rGO	39.4	0.0008–12.78	0.5	[45]
Ag-Au/Cu_2O/GCE	4.16	0-1.4	1.3	[46]
Cu_2O Hexapods /Nafion/GCE	94.4	0.05-3.6	5.4	[18]
CuO/Ag	NR	0.05-0.5	4	[47]
Cu_2O Cubes/GCE	25	0.5-8500	1.61	[40]
PdNPs-CNT/GCE	68	0.02-1	14	[48]
AuNBP/CNTs	170.6	0.005-47.3	1.5	[49]
Co-Al /CNT	118	0.1-4	10	[50]
NiMn-LDH/GO	96.82	0.02-8.65	4.4	[51]
$CuCo_2O_4$/GCE	400	0.01-8.9	3	[52]
$NiCo_2S_4$/rGO	118.5	0.025-11.25	0.19	[53]
Cu_2O spheres - CNT (RDE at 800 RPM)	642	0.007-5	1	This work
Cu_2O spheres - CNT (In quiescent solutions)	162	0.050-10	50	This work

Table 2. Analytical performance comparison of various hydrogen peroxide electrochemical sensors. GO: Oxide graphene; rGO: reduced graphene oxide; NBP: nanobipyramids; LDH: Layered double hydroxides.

Summing up, the preparation of a CNT/Cu_2O inks showed promising results as the catalytic properties of cuprous oxide particles were preserved while carbon nanotubes provide mechanical stability and electrical conductivity suitable for the development of printed devices. Electrocatalytic non-enzymatic electrodes could be fabricated by printing a single layer of ink. The use of spheres would be the most suitable to develop a non-enzymatic printed sensor to detect H_2O_2 as they present both high sensitivity and stability among the tested cuprous oxide morphologies.

Conclusions

A simple and surfactant-free method for the synthesis of cuprous oxide mesoparticles has been developed. The morphology of cuprous oxide particles could be controlled by simply varying the ratio of three reactants at room temperature. Seven different particle morphologies have been obtained using this method. The particles were incorporated into a waterborne CNT ink which was used for the fabrication of electrodes with electrocatalytic activity towards hydrogen peroxide reduction onto a flexible substrate thus combining electrical conduction and catalytic activity in a single printed layer. A sensitivity of 162 µA cm^{-2} mM^{-1} and a limit of detection of 50 µM were obtained for an amperometric sensor made with the carbon nanotube ink containing spherical cuprous oxide particles in quiescent solutions.

Acknowledgements

We thank INTI, ANPCyT (PICT 2013-0427, PICT 2014-3748 and PICT 2017-2787) and CONICET (PIP 11220150100967) for financial support. Authors are also grateful to Anahí Medrano for the preparation of the inks. LNM is research staff of CONICET.

References

[1] Tian, N., Zhou, Z. Y. & Sun, S. G. Platinum metal catalysts of high-index surfaces: from single-crystal planes to electrochemically shape-controlled nanoparticles. J. Phys. Chem. C 112, 19801–19817 (2008).

[2] Tao, A. R., Habas, S. & Yang, P. Shape control of colloidal metal nanocrystals. Small 4, 310–325 (2008).

[3] Mikami, K., Kido, Y., Akaishi, Y., Quitain, A. & Kida, T. Synthesis of Cu_2O/CuO nanocrystals and their application to H2S sensing. Sensors 19, (2019).

[4] Zhou, D. L. et al. Facile synthesis of monodisperse porous Cu_2O nanospheres on reduced graphene oxide for non-enzymatic amperometric glucose sensing. Electrochim. Acta 115, 103–108 (2014).

[5] Jina, J., Meia, H., Wua, H., Wanga, S., Xia, Q., Ding, Y. Selective detection of dopamine based on Cu_2O@Pt core-shell nanoparticles modified electrode in the presence of ascorbic acid and uric acid. J. Alloys Compd. 784, 827–833 (2019)

[6] Huang, Y. et al. Synthesis of CuO/g-C_3N_4 composites, and their application to voltammetric sensing of glucose and dopamine. Electrochim. Acta 186, 10 (2018).

[7] Ho, J. Y. & Huang, M. H. Synthesis of submicrometer-sized Cu_2O crystals with morphological evolution from cubic to hexapod structures and their comparative photocatalytic activity. J. Phys. Chem. C 113, 14159–14164 (2009).

[8] Aguirre, E., Zhou, R., Eugene, A. J., Guzman, M. I. & Grela, A. Cu_2O/TiO_2 heterostructures for CO_2 reduction through a direct Z-scheme: Protecting Cu_2O from photocorrosion. "Applied Catal. B, Environ. 217, 485–493 (2017).

[9] Ma, Q. B., Hofmann, J. P., Litke, A. & Hensen, E. J. M. Cu_2O photoelectrodes for solar water splitting: Tuning photoelectrochemical performance by controlled faceting. Sol. Energy Mater. Sol. Cells 141, 178–186 (2015).

[10] Zhang, Z. et al. Facile synthesis of mesoporous Cu_2O microspheres with improved catalytic property for dimethyldichlorosilane synthesis. Ind. Eng. Chem. Res. 51, 1264–1274 (2012).

[11] Xu, Y. et al. Cu_2O nanocrystals: Surfactant-free room-temperature morphology-modulated synthesis and shape-dependent heterogeneous organic catalytic activities. J. Phys. Chem. C 115, 15288–15296 (2011).

[12] McFadyen, P. & Matijević, E. Copper Hydrous Oxide Sols of Uniform Particle Shape and Size. J. Inorg. Nucl. Chem. 35, (1973).

[13] Zhang, D. F. et al. Delicate control of crystallographic facet-oriented Cu_2O nanocrystals and the correlated adsorption ability. J. Mater. Chem. 19, 5220–5225 (2009).

[14] Wang, X., Chen, M., He, Y. & Zhu, J. Shape-controlled preparation of Cu_2O crystals and their growth mechanism. J. Alloys Compd. 628, 50–56 (2015).

[15] Gou, L. & Murphy, C. J. Controlling the size of Cu_2O nanocubes from 200 to 25 nm. J. Mater. Chem. 14, 735–738 (2004).

[16] Gou, L. & Murphy, C. J. Solution-Phase Synthesis of Cu_2O Nanocubes. Nano Lett. 3, 231–234 (2003).

[17] Kuo, C. H. & Huang, M. H. Facile synthesis of Cu_2O nanocrystals with systematic shape evolution from cubic to octahedral structures. J. Phys. Chem. C 112, 18355–18360 (2008).

[18] Zhong, Y., Li, Y., Li, S. & Zhang, Y. Nonenzymatic hydrogen peroxide biosensor based on four different morphologies of cuprous oxide nanocrystals. RSC Adv. 4, 40638–40642 (2014).

[19] Wang, Z., Wang, H., Wang, L. & Pan, L. Controlled synthesis of Cu_2O cubic and octahedral nano- and microcrystals. Cryst. Res. Technol. 44, 624–628 (2009).

[20] Ke, W. H., Hsia, C. F., Chen, Y. J. & Huang, M. H. Synthesis of Ultrasmall Cu_2O Nanocubes and Octahedra with Tunable Sizes for Facet-Dependent Optical Property Examination. Small 12, 3530–3534 (2016).

[21] Wang, Y. & Zhou, K. Effect of OH^- on morphology of Cu_2O particles prepared through reduction of Cu(II) by glucose. J. Cent. South Univ. 19, 2125–2129 (2012).

[22] Huang, W. C., Lyu, L. M., Yang, Y. C. & Huang, M. H. Synthesis of Cu_2O nanocrystals from cubic to rhombic dodecahedral structures and their comparative photocatalytic activity. J. Am. Chem. Soc. 134, 1261–1267 (2012).

[23] Lan, X., Zhang, J., Gao, H. & Wang, T. Morphology-controlled hydrothermal synthesis and growth mechanism of microcrystal Cu_2O. CrystEngComm 13, 633–636 (2011).

[24] Xu, H., Wang, W. & Zhu, W. Shape Evolution and Size-Controllable Synthesis of Cu_2O Octahedra and Their Morphology-Dependent Photocatalytic Properties. J. Phys. Chem. B 110, 13829–13834 (2006).

[25] Susman, M. D., Feldman, Y., Vaskevich, A. & Rubinstein, I. Chemical Deposition of Cu_2O Nanocrystals with Precise Morphology. ACS Nano 8, 162–174 (2014).

[26] Zhao, X., Bao, Z., Sun, C. & Xue, D. Polymorphology formation of Cu_2O: A microscopic understanding of single crystal growth from both thermodynamic and kinetic models. J. Cryst. Growth 311, 711–715 (2009).

[27] Kim, M. H., Lim, B., Lee, E. P. & Xia, Y. Polyol synthesis of Cu_2O nanoparticles: Use of chloride to promote the formation of a cubic morphology. J. Mater. Chem. 18, 4069–4073 (2008).

[28] Dhara, K. & Mahapatra, D. R. Recent advances in electrochemical nonenzymatic hydrogen peroxide sensors based on nanomaterials: a review. J. Mater. Sci. 54, 12319–12357 (2019).

[29] Giorgio, M., Trinei, M., Migliaccio, E. & Pelicci, P. G. Hydrogen peroxide: A metabolic by-product or a common mediator of ageing signals? Nat. Rev. Mol. Cell Biol. 8, 722–728 (2007).

[30] Wilson, R. & Elizabeth, Q. Glucose oxidase : An ideal enzyme. *Biosens. Bioelectron.* 5663, 165–185 (2016).

[31] Goran, J. M., Lyon, J. L. & Stevenson, K. J. Amperometric detection of l-lactate using nitrogen-doped carbon nanotubes modified with lactate oxidase. Anal. Chem. 83, 8123–8129 (2011).

[32] Li, Z., Sheng, L., Meng, A., Xie, C. & Zhao, K. A glassy carbon electrode modified with a composite consisting of reduced graphene oxide, zinc oxide and silver nanoparticles in a chitosan matrix for studying the direct electron transfer of glucose oxidase and for enzymatic sensing of glucose. Microchim. Acta 183, 1625–1632 (2016).

[33] Li, S. et al. Enzyme-free amperometric sensing of hydrogen peroxide and glucose at a hierarchical Cu_2O modified electrode. Talanta 85, 1260–1264 (2011).

[34] Moro, G. et al. Disposable electrodes from waste materials and renewable sources for (bio)electroanalytical applications. Biosens. Bioelectron. 146, 111758 (2019).

[35] Sui, Y. & Zorman, C. A. Inkjet Printing of Metal Structures for Electrochemical Sensor Applications: A Review. J. Electrochem. Soc. 167, 037571 (2020).

[36] Jiang, Y. & Zhu, N. Flexible and Printed Electronics for Smart Clothes. In “Flexible and Wearable Electronics for Smart Clothing”, pp. 253-284. Ed. Gang Wang, Chengyi Hou, Hongzhi Wang. Wiley-VCH Verlag GmbH& Co. KGaA, Weinheim, Germany, 2020.

[37] Garate, O. et al. Waterborne carbon nanotube ink for the preparation of electrodes with applications in electrocatalysis and enzymatic biosensing. Mater. Res. Bull. 106, 137–143 (2018).

[38] Molinari, J., Florez, L., Medrano, A., Monsalve, L. & Ybarra, G. Electrochemical determination of β-lactoglobulin employing a polystyrene bead-modified carbon nanotube ink. Biosensors 8, 3–11 (2018).

[39] Garate, O. et al. Waterborne carbon nanotube ink for the preparation of electrodes with applications in electrocatalysis and enzymatic biosensing. Mater. Res. Bull. 106, 137–143 (2018).

[40] Meng, L. et al. Synthesis and size-dependent electrochemical nonenzymatic H_2O_2 sensing of cuprous oxide nanocubes. RSC Adv. 5, 82496–82502 (2015).

[41] Xu, J. & Xue, D. Five branching growth patterns in the cubic crystal system: A direct observation of cuprous oxide microcrystals. Acta Mater. 55, 2397–2406 (2007).

[42] Shang, Y. & Guo, L. Facet-Controlled Synthetic Strategy of Cu_2O-Based Crystals for Catalysis and Sensing. Adv. Sci. 2, (2015).

[43] Sun, S. et al. Etching-limited branching growth of cuprous oxide during ethanol-assisted solution synthesis. CrystEngComm 13, 2837–2840 (2011).

[44] Zhang, L. & Wang, H. Cuprous Oxide Nanoshells with Geometrically Tunable Optical Properties. ACS Nano 5, 3257–3267 (2011).

[45] Liu, J. et al. Preparation of a nanocomposite material consisting of cuprous oxide, polyaniline and reduced graphene oxide, and its application to the electrochemical determination of hydrogen peroxide. Microchim. Acta 185, 1–8 (2018).

[46] Li, D., Meng, L., Dang, S., Jiang, D. & Shi, W. Hydrogen peroxide sensing using Cu_2O nanocubes decorated by Ag-Au alloy nanoparticles. J. Alloys Compd. 690, 1–7 (2017).

[47] Hooch Antink, W., Choi, Y., Seong, K. dong & Piao, Y. Simple synthesis of CuO/Ag nanocomposite electrode using precursor ink for non-enzymatic electrochemical hydrogen peroxide sensing. Sensors Actuators, B Chem. 255, 1995–2001 (2018).

[48] Hamidi, H. & Haghighi, B. Fabrication of a sensitive amperometric sensor for NADH and H_2O_2 using palladium nanoparticles-multiwalled carbon nanotube nanohybrid. Mater. Sci. Eng. C 62, 423–428 (2016).

[49] Mei, H. et al. A nanocomposite consisting of gold nanobipyramids and multiwalled carbon nanotubes for amperometric nonenzymatic sensing of glucose and hydrogen peroxide. Microchim. Acta 186, (2019).

[50] Heli, H., Pishahang, J. & Amiri, H. B. Synthesis of hexagonal CoAl-layered double hydroxide nanoshales/carbon nanotubes composite for the non-enzymatic detection of hydrogen peroxide. J. Electroanal. Chem. 768, 134–144 (2016).

[51] Zhou, J., Min, M., Liu, Y., Tang, J. & Tang, W. Layered assembly of NiMn-layered double hydroxide on graphene oxide for enhanced non-enzymatic sugars and hydrogen peroxide detection. Sensors Actuators, B Chem. 260, 408–417 (2018).

[52] Cheng, D., Wang, T., Zhang, G., Wu, H. & Mei, H. A novel nonenzymatic electrochemical sensor based on double-shelled $CuCo_2O_4$ hollow microspheres for glucose and H_2O_2. J. Alloys Compd. 819, 153014 (2020).

[53] Wang, M. et al. A novel H_2O_2 electrochemical sensor based on $NiCo_2S_4$ functionalized reduced graphene oxide. J. Alloys Compd. 784, 827–833 (2019).

Journal of Alloys and Compounds:" Performance of Cuprous Oxide Mesoparticles with Different Morphologies as Catalysts in a Carbon Nanotube Ink for Printing Electrochemical Sensors"

- A facile surfactant-free synthetic route is presented to obtain Cu_2O particles of different morphologies by varying the concentration of only three reactants.
- The influence of the reactants in the growth mechanism has been discussed.
- A carbon nanotube and Cu_2O ink has been formulated for the preparation of printable electrodes for the electrochemical detection of H_2O_2.
- The electrochemical sensor presents a high sensitivity and a low limit of detection.

Declaration of interests

☒ The authors declare that they have no known competing financial interests or personal relationships that could have appeared to influence the work reported in this paper.

☐The authors declare the following financial interests/personal relationships which may be considered as potential competing interests: